The Journal of Prevention of Alzheimer's Disease 13 (2026) 100639

Contents lists available at ScienceDirect

The Journal of Prevention of Alzheimer's Disease

journal homepage: www.elsevier.com/locate/tjpad

Original Article

Glymphatic dysfunction, plasma neurofilament light, and cortical free water mediate cognitive decline in familial frontotemporal lobar degeneration

Meiling Qiu [a,b,1], Li Ding [a,b,1], Rui Bao [a,c,1], Juanyu Gong [a,c], Wencai Ding [a,c,**], Zhiding Shao [a,c,**], Yongsheng Han [a,*], for the ARTFL-LEFFTDS Longitudinal Frontotemporal Lobar Degeneration (ALLFTD) Research Consortium[1]

[a] *Wannan Medical University, Wuhu, 241000, China*
[b] *The First Affiliated Hospital of Wannan Medical University, Wuhu, 241000, China*
[c] *The Second Affiliated Hospital of Wannan Medical University, Wuhu, 241000, China*

ARTICLE INFO

Keywords:
f-FTLD
Glymphatic system
DTI-ALPS
Cortical free water
NfL

ABSTRACT

Background: Familial frontotemporal lobar degeneration (f-FTLD) is the second most common form of young-onset dementia, with diverse clinical presentations, neuropathological substrates and genetic backgrounds. While evidence suggests that glymphatic dysfunction, neuroaxonal injury, and cortical microstructural alterations may jointly contribute to f-FTLD, their interrelationships across genotypes remain unclear.
Objectives: This study aims to investigate the roles of glymphatic dysfunction, cortical free water (cFW), and plasma neurofilament light (NfL) in f-FTLD and examine their relationship with cognitive decline.
Design: A multimodal approach was applied, involving diffusion tensor imaging along the perivascular space (DTI-ALPS) for glymphatic function, plasma NfL measurement, and voxel-wise cortical free water mapping. Analyses comparing FTLD mutation groups and serial mediation analyses were conducted in 322 participants (*C9orf72, GRN, MAPT* mutation carriers, and matched controls).
Setting: This study was conducted across multiple participating centers using standardized imaging protocols and harmonized multi-site data.
Participants: A total of 322 participants were included: 87 *C9orf72* expansion carriers, 56 *GRN* mutation carriers, 58 *MAPT* mutation carriers, and 121 healthy controls.
Intervention: No intervention was applied in this observational study. Participants underwent genetic testing, cognitive assessment, and diffusion MRI scans; plasma NfL was available for mutation carriers.
Measurements: Glymphatic function was assessed using DTI-ALPS, plasma NfL levels were measured to reflect neuroaxonal injury, and cortical microstructure was assessed through cortical free water (cFW) mapping.
Results: Significant reductions in DTI-ALPS and elevations in cFW were observed in *C9orf72* and *GRN* mutation carriers, with strong associations to clinical cognitive decline. Plasma NfL levels were highest in *GRN* mutation carriers and correlated strongly with cognitive severity. Mediation analysis indicated that the pathway linking DTI-ALPS to cognition through NfL explained a substantial portion of the indirect effect, while residual direct effects suggested that additional mechanisms also contribute to cognitive decline.
Conclusions: This study identifies glymphatic dysfunction as a key factor contributing to cognitive decline in f-FTLD, with plasma NfL serving as an important partial mediator and cFW providing additional region-specific information.

* Corresponding authors at: Wannan Medical University, Wuhu, 241000, China.
** Corresponding authors at: The Second Affiliated Hospital of Wannan Medical University, Wuhu, 241000, China.
E-mail addresses: dingneurology@wnmc.edu.cn (W. Ding), 20122087@wnmc.edu.cn (Z. Shao), hyssp@126.com (Y. Han).
[1] These authors contributed equally to this work.

https://doi.org/10.1016/j.tjpad.2026.100639
Received 12 February 2026; Received in revised form 30 May 2026; Accepted 24 June 2026
Available online 4 July 2026
2274-5807/© 2026 The Authors. Published by Elsevier Masson SAS on behalf of SERDI Publisher. This is an open access article under the CC BY-NC-ND license (http://creativecommons.org/licenses/by-nc-nd/4.0/).

1. Introduction

Frontotemporal lobar degeneration (FTLD) represents the second most common form of young-onset dementia, with diverse clinical presentations, neuropathological substrates, and genetic backgrounds [1]. Across FTLD subtypes, cortical microstructural changes often precede overt cortical atrophy [2,3]. Approximately 30% of cases arise from autosomal dominant pathogenic variants, defining familial FTLD (f-FTLD). The majority of these inherited cases are caused by mutations in *C9orf72*, microtubule-associated protein tau (*MAPT*), or granulin precursor (*GRN*) [4–6]. Our recent findings show that microstructural alterations emerge before cortical atrophy in all three genetic subtypes [7], indicating that such changes are closely linked to the pathological proteins underlying FTLD.

Increasing evidence implicates impaired interstitial fluid clearance in the pathogenesis of neurodegeneration. The glymphatic pathway enables cerebrospinal fluid to interact with interstitial fluid through perivascular channels, a process modulated by aquaporin-4 on astrocytic endfeet, and subsequently cleared via arachnoid granulations and meningeal lymphatic routes [5,8–12]. Diffusion MRI offers a noninvasive approach to estimate glymphatic function, most commonly via the diffusion tensor imaging–along the perivascular space (DTI-ALPS) index. Prior studies reported markedly lower DTI-ALPS indices in FTLD compared with controls, with regional reductions linked to cognitive impairment [13,14]. In Alzheimer's disease (AD), disrupted glymphatic function has further been implicated in cortical microstructural damage [15]. Such injury, including neuronal loss and synaptic disintegration, expands the extracellular space and manifests on MRI as increased free water (FW) [16]. FW elevations can occur before cortical atrophy and are independently associated with faster cognitive decline [17,18]. Similarly, elevated plasma neurofilament light chain (NfL), a sensitive marker of axonal injury, reflects neuronal loss even in early disease stages [19].

Converging evidence suggests that impaired glymphatic clearance and cortical microstructural disruption act together to drive axonal injury and cognitive decline. DTI-ALPS studies in genetic FTLD have shown that reduced glymphatic function is linked to vascular dysfunction and astrocytic activation, pointing to possible genotype-specific effects [12,20]. At the molecular level, plasma NfL is a sensitive marker of axonal injury and strongly correlates with disease progression [19]. If glymphatic failure leads to accumulation of toxic proteins or metabolites, this process may accelerate axonal damage, trigger MRI-detectable microstructural changes, and ultimately worsen cognition. NfL is therefore a plausible mediator between impaired clearance and structural brain injury. However, it remains unclear whether these pathways are shared across *C9orf72, MAPT*, and *GRN* subtypes or whether they vary by brain region. Addressing this knowledge gap requires multimodal mediation analyses across specific FTLD mutation groups.

To bridge these knowledge gaps, we examined a substantial cohort of genetically verified f-FTLD patients alongside matched healthy controls, applying a multimodal framework. All participants underwent genetic testing, comprehensive neuropsychological assessment, plasma NfL measurement, and dMRI to evaluate glymphatic function with DTI-ALPS and cortical microstructure with voxel-wise FW mapping. We then applied chain-mediation analyses to test whether impaired glymphatic clearance contributes to cognitive decline through elevated NfL and region-specific FW, and whether these pathways differ across cortical regions. To the best of our knowledge, this represents the first attempt to combine ALPS, FW, and NfL within a mediation framework performed for each genetic subtype in f-FTLD. Clarifying these mechanisms may improve early detection and support biomarker development for therapeutic monitoring in familial FTLD.

2. Materials and methods

2.1. Ethics

All data were obtained in de-identified form from participating study centers, which ensured compliance with institutional and national ethical standards. All participants provided written informed consent. The study protocol was reviewed and approved by the local Institutional Review Boards and complied with the principles of the Declaration of Helsinki (see Acknowledgment statement).

2.2. Study participants

Enrollment was carried out via the ALLFTD consortium, including both symptomatic and presymptomatic carriers of pathogenic variants in the three major FTLD-related genes (*C9orf72, MAPT* and *GRN*) [21]. The study included 322 individuals: 87 *C9orf72* expansion carriers, 58 *MAPT* mutation carriers, 56 *GRN* mutation carriers, and 121 noncarrier family members. FTLD diagnosis was made using established consensus clinical guidelines and further verified by genetic testing [22]. All healthy controls were non-carrier family members from the ALLFTD cohort who tested negative for pathogenic FTLD mutations, had no history of neurological or psychiatric disorders, and were matched to mutation carriers on age and sex. Mutation carriers were classified as pre-symptomatic carriers (pre-Sx) if CDR® plus NACC FTLD = 0 and as symptomatic carriers (Sx) if CDR® plus NACC FTLD > 0.

2.3. Neuropsychological assessment

Disease severity was assessed using the Clinical Dementia Rating scale plus National Alzheimer's Coordinating Center Frontotemporal Lobar Degeneration module (CDR® plus NACC FTLD), a validated measure for standardized assessment of cognitive and functional decline in FTLD [23]. This instrument extends the traditional CDR framework by incorporating FTLD-relevant behavioral, language, and executive domains, which are central to FTLD but may not be fully captured by global cognitive screening measures alone.

2.4. Plasma NfL

Plasma NfL levels were measured on a Quanterix HD-X Analyzer in duplicate, following the manufacturer's instructions. Blood was collected in EDTA-coated tubes, centrifuged at 1500 × g for 15 min at 4 °C, aliquoted, and stored at −80 °C until analysis. All samples were assayed in duplicate on a Quanterix HD-X Analyzer following the manufacturer's protocol. Internal standards and duplicate measures were included in each run to ensure assay reliability.

2.5. Genetic testing

All participants underwent genotyping for *C9orf72, MAPT*, and *GRN* mutations associated with FTLD [22]. Clinical-grade genetic testing was offered to all participants, although most asymptomatic carriers declined. Study clinicians were blinded to mutation status unless results had already been disclosed to the participant [23].

2.6. Neuroimaging data acquisition

All MRI images were acquired using 3T scanners equipped with an 8-channel phased-array head coil. High-resolution T1-weighted images were acquired using a 3D magnetization-prepared rapid gradient echo sequence. Diffusion tensor imaging was performed in the axial plane using a single-shot echo-planar imaging sequence with 48 diffusion-weighted directions at b = 1000 s/mm^2, 6 non-diffusion-weighted b0 volumes, and 2.7-mm isotropic resolution. Detailed acquisition parameters are provided in the Supplementary Materials.

2.7. Neuroimaging data processing

2.7.1. T1 imaging

T1-weighted images were processed with the FreeSurfer cross-sectional pipeline (v7.4.1). Cortical thickness was estimated as the distance between the gray–white matter interface and the pial surface. All segmentations were visually checked for accuracy. Thickness maps were aligned to the fsaverage template using spherical registration and smoothed with a 10-mm full-width at half maximum (FWHM) Gaussian kernel.

2.8. DTI imaging

2.8.1. Cortical microstructure—Free water

DMRI was processed using a customized surface-based pipeline integrating FSL (version 6.0.4) and FreeSurfer (version 7.4.1). Scans with motion exceeding 2 mm or 2° were excluded, and data were corrected for eddy currents, head motion, and susceptibility distortions [24]. Free water (FW) maps were derived using a bi-tensor model. This approach was chosen because MRI-derived free water has been evaluated as a multicenter imaging biomarker in the MarkVCID consortium [25,26]. FW maps were registered to individual T1-weighted images using boundary-based registration, sampled at 50% cortical depth, projected to the cortical surface, aligned to the fsaverage template, and smoothed with a 10-mm Gaussian kernel [27]. Mean cortical FW (cFW) values were extracted globally across the cortical mantle and regionally from FTLD-vulnerable cortical regions selected a priori based on established patterns of frontotemporal degeneration. Specifically, bilateral cFW values were averaged for five Desikan–Killiany atlas regions: caudal middle frontal cortex, frontal pole, temporal pole, insula, and isthmus cingulate cortex [28–30]. These regions were selected to represent frontal, anterior temporal, insular, and cingulate components of the FTLD-vulnerable network.

2.8.2. DTI-ALPS analysis

Glymphatic function was assessed with the DTI-ALPS approach as described by Taoka et al. [16]. ROIs were positioned on projection and association fiber regions adjacent to the body of the lateral ventricle at the corona radiata level, where perivascular spaces are oriented mainly along the x-axis. Diffusivities were sampled along x (Dx), y (Dy), and z (Dz) directions for projection and association fibers, and the DTI-ALPS index was defined as:

$$\mathrm{DTI-ALPS} = \frac{\mathrm{mean}(\mathrm{Dx-proj},\quad \mathrm{Dx-assoc})}{\mathrm{mean}(\mathrm{Dy-proj},\quad \mathrm{Dz-assoc})}$$

The DTI-ALPS index was calculated as the ratio of diffusivity along perivascular pathways to that in orthogonal directions. Higher values indicate relatively preserved perivascular fluid movement.

Bilateral spherical ROIs (3 mm) were positioned within perivascular areas of the superior longitudinal fasciculus (association fibers) and the upper/posterior corona radiata (projection fibers). ROIs were initially defined in Montreal Neurological Institute (MNI) standard space and transformed to T1 space using a nonlinear deformation matrix derived from the Human Connectome Project (HCP) 1065-subject fractional anisotropy (FA) template, implemented with the *antsRegistrationSyNQuick.sh* function in Advanced Normalization Tools (ANTs, version 2.2.0; http://stnava.github.io/ANTs). ROIs were subsequently registered to each individual's T1 space using FA-to-T1 transformation. Coordinates were refined to align with perivascular spaces, accounting for anatomical variability, and placements were confirmed independently by two raters. The complete analytic pipeline is illustrated in Graphical Abstract (Supplementary Materials).

2.9. Statistical analysis

All statistical analyses were conducted using R (version 4.4.2). Normality was assessed using the Shapiro–Wilk test. Normally distributed continuous variables are presented as mean ± standard deviation, whereas non-normally distributed variables are presented as median and interquartile range. Categorical variables are summarized as male: female ratios. Between-group comparisons were performed using independent-sample t tests for normally distributed variables and Mann–Whitney U tests for non-normally distributed variables when pairwise comparisons were conducted. Chi-square or Fisher's exact tests were used for categorical variables. All tests were two-tailed, and statistical significance was set at $P < 0.05$.

Imaging metrics (cFW and DTI-ALPS) were compared between groups using independent *t*-tests, with FDR correction applied at $P < 0.05$. To reduce scanner/site variability, imaging data were harmonized across centers using ComBat (neuroCombat) with age and sex included as covariates [31].

Surface-based regression analyses were conducted to evaluate associations among cortical free-water fraction (cFW), DTI-ALPS, plasma NfL, and CDR® plus NACC FTLD scores, controlling for age, sex, and education. Analyses were restricted to cortical gray matter. For global summary measures, associations were assessed using correlation methods appropriate to the underlying data distribution, and analyses were repeated in symptomatic carriers to ensure robustness of findings.

Mediation analyses were performed to examine whether cFW and plasma NfL mediated the relationship between DTI-ALPS and cognition (CDR® plus NACC FTLD). Two sequential models were tested: in Model A, DTI-ALPS predicted cFW, which then predicted NfL, and both variables were specified as mediators of cognition; in Model B, DTI-ALPS predicted NfL, which then predicted cFW, with both variables serving as sequential mediators. Both models were evaluated, and subsequent regional interpretation focused on the model showing the more robust and biologically interpretable indirect pathway. For each model, direct effects (c' path), indirect effects through individual mediators, sequential indirect effects, and total effects were estimated. All continuous variables were z-standardized prior to analysis. Structural equation modeling was implemented in R (lavaan package, version 0.6–1.1240) with maximum likelihood estimation and 1000 bootstrap replications to generate bias-corrected confidence intervals. Indirect effects were deemed significant when the 95% confidence interval did not cross zero. Analyses were performed both at the whole-brain cFW level and within FTLD-vulnerable cortical regions defined by the Desikan–Killiany atlas, averaging left and right hemisphere values for each region.

To minimize the potential influence of pre-symptomatic carriers on disease severity–related associations, the correlation and mediation analyses were repeated in symptomatic carriers (Sx).

3. Results

3.1. Participant characteristics

The study included 322 participants: 87 C9orf72 expansion carriers, 56 GRN mutation carriers, 58 MAPT mutation carriers, and 121 healthy controls. Among mutation carriers, 35 C9orf72, 22 GRN, and 18 MAPT carriers were symptomatic, defined as CDR® plus NACC FTLD > 0. Sex distribution and education were comparable across groups, whereas age differed by genotype, with GRN carriers being older and MAPT carriers being relatively younger (Table 1.).

Clinical severity was minimal in the full carrier groups because Pre-Sx and Sx individuals were both included, but CDR® plus NACC FTLD scores were clearly elevated in symptomatic carriers across all three genetic subtypes. For imaging markers, DTI-ALPS was reduced in C9orf72 carriers, especially in the symptomatic subgroup, while cFW was elevated in C9orf72 and GRN carriers compared with MAPT carriers and healthy controls. Plasma NfL was available only in genetic carriers

Table 1
Demographic, neuroimaging, and clinical characteristics across FTLD genetic subtypes and healthy controls.

	N	Sex, M:F	Age, y	EDU, y	DTI-ALPS	cFW	CDR® plus NACC FTLD	NfL (pg/ml)
C9orf72(All)	87	39: 48	50 (38–60)	16 (14–18)	1.45± 0.24*	0.58 (0.57–0.59)***	0 (0–2)***	8.97 (5.13–17.5)
C9orf72(Sx)	35	17: 18	57 (50.5–62.5)**	16 (14–17.5)	1.32±0.21***	0.58 (0.58–0.59)***	4.5 (1.5–6.75)***	19.1 (10.1–40.7)
GRN(All)	56	27: 29	59.5 (45.5–66)**	16 (13.8–18)	1.47± 0.24	0.58 (0.57–0.59)***	0 (0–3.62)***	10.6 (5.23–41.1)
GRN(Sx)	22	9: 13	63.5 (58.5–67.8)***	14 (12.2–16)	1.36±0.247**	0.58 (0.58–0.59)***	4.75 (3.12–8.75)***	54.2 (33.6–80.9)
MAPT(All)	58	27: 31	43.5 (33.5–52.8)*	16 (14–17.8)	1.56± 0.25	0.30 (0.28–0.34)	0 (0–1.5)**	6.95 (4.23–13.30)
MAPT(Sx)	18	9: 9	56 (49–60.8)	16 (14–17.8)	1.42±0.275	0.37 (0.34–0.49)***	5.25 (2–7)***	14.8 (12.7–21.6)
HC	121	50: 71	50 (37–58)	16 (13–18)	1.53±0.22	0.30 (0.28–0.33)	0 (0–0)	
P-value								
C9orf72 vs. GRN		0.73	0.82	0.92	0.48	0.89	0.331	0.81
GRN vs. MAPT		1.00	<0.001	0.92	0.12	<0.001	0.085	0.39
C9orf72 vs MAPT		0.87	0.972	0.92	0.03	<0.001	0.310	0.39

Demographic, neuroimaging, and clinical characteristics across frontotemporal lobar dementia (FTLD) genetic subtypes and healthy controls (HC). C9orf72, chromosome 9 open reading frame 72; GRN, progranulin; MAPT, microtubule-associated protein tau; HC, healthy controls; All, all mutation carriers within each genetic subtype; Sx, symptomatic carriers, defined as CDR® plus NACC FTLD > 0; N, number of participants; M:F, male:female ratio; y, years; EDU, years of education; DTI-ALPS, diffusion tensor image analysis along the perivascular space; cFW, cortical free water fraction; CDR, Clinical Dementia Rating scale; NfL, plasma neurofilament light chain. DTI-ALPS is presented as mean ± standard deviation, whereas age, education, cFW, CDR® plus NACC FTLD, and NfL are presented as median (interquartile range). Sex is presented as a male:female ratio. P-values in the lower rows indicate pairwise comparisons among FTLD genetic subtypes. Superscript asterisks indicate comparisons with HC: $*P < 0.05$, $**P < 0.01$, $***P < 0.001$. Plasma NfL data were not available for HC; therefore, NfL comparisons were performed only among genetic subtypes.

and was highest in GRN carriers, particularly among symptomatic individuals. These findings indicate that although the cohort was broadly balanced for sex and education, it showed clear genotype- and stage-related differences in age, disease severity, cFW, DTI-ALPS, and NfL levels (Table 1 and Figure S1).

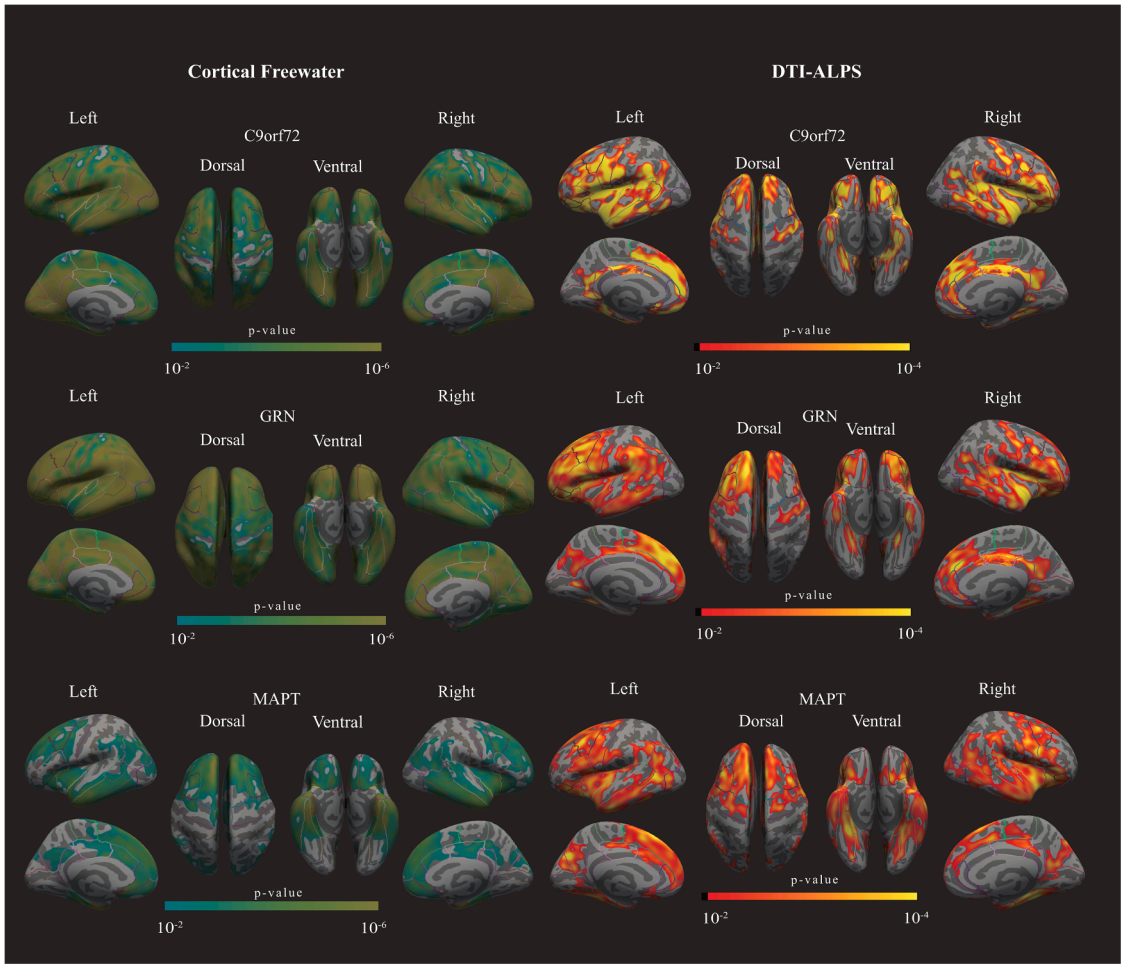

Fig. 1. Group differences in cortical FW and DTI-ALPS index between familial FTLD genetic subtypes (C9orf72, GRN, MAPT) and healthy controls. Group differences in cortical FW and DTI-ALPS index between familial FTLD genetic subtypes (C9orf72, GRN, MAPT) and healthy controls. Left panel: cortical FW vertex-wise p-value maps from pairwise comparisons between each FTLD mutation group and healthy controls. Right panel: DTI-ALPS vertex-wise p-value maps from the corresponding pairwise comparisons. Color intensity represents the magnitude of the vertex-wise p-values and does not indicate that all displayed regions survived correction. Group comparisons were adjusted for age, sex, and center, and corrected statistical significance was set at $P < 0.01$.

3.2. Group differences in cFW and DTI-ALPS among FTLD genetic subtypes and controls

Between-group comparisons indicated that cFW in MAPT carriers did not differ significantly from healthy controls, whereas cFW was markedly elevated in C9orf72 and GRN carriers relative to both MAPT carriers and healthy controls. By comparison, both the C9orf72 and GRN subtypes each demonstrated significant cFW differences relative to healthy controls. In the full mutation-carrier groups, DTI-ALPS was significantly reduced in C9orf72 carriers relative to healthy controls and differed between C9orf72 and MAPT carriers, whereas GRN and MAPT carriers did not differ significantly from controls. In the Sx subgroup, both C9orf72 and GRN carriers showed lower DTI-ALPS relative to healthy controls. For cFW, C9orf72 and GRN carriers showed marked elevations in the full carrier groups, whereas MAPT carriers showed relatively lower cFW in the full-group comparison; however, MAPT symptomatic carriers also showed elevated cFW relative to healthy controls.

Vertex-wise p-value maps showed widespread cFW differences in C9orf72 and GRN carriers compared with controls. In MAPT carriers, the spatial pattern was more restricted and did not correspond to a significant global cFW difference from controls (Fig. 1). Spatial patterns of DTI-ALPS also varied by genotype: C9orf72 carriers showed reductions primarily in the bilateral frontal and temporal lobes, extending to the supramarginal and precentral gyri and, to a lesser extent, the parietal and cingulate cortices. GRN carriers exhibited more widespread reductions, particularly in the frontal lobes. In contrast, *MAPT* carriers showed a relatively restricted distribution of DTI-ALPS decline, with focal involvement in the superior frontal gyrus, fusiform gyrus, and precentral gyrus. (Fig. 1)

3.3. Associations of cFW, DTI-ALPS, and NfL with cognition

Across the full cohort, significant associations were observed between imaging and fluid biomarkers and clinical severity. The DTI-ALPS index correlated negatively with CDR® plus NACC FTLD ($r = –0.413$, $P < 0.0001$) (Fig. 2A.). In contrast, cFW correlated positively ($r = 0.221$, $P = 0.002$), as did plasma NfL ($r = 0.517$, $P < 0.0001$) (Fig. 3B). To assess whether these associations were driven by Pre-Sx carriers, the correlation analyses were repeated in Sx carriers only. The overall direction of the associations was broadly consistent with the primary analysis, although the effect sizes were attenuated after restricting the sample to symptomatic individuals. In Sx-only analyses, the DTI-ALPS index remained negatively associated with CDR® plus NACC FTLD ($r = −0.296$, $P = 0.010$), and plasma NfL remained positively associated with clinical severity ($r = 0.323$, $P = 0.005$). The association between cFW and CDR® plus NACC FTLD was attenuated and did not reach statistical significance in Sx carriers ($r = 0.184$, $P = 0.115$).

Region-wise cFW–cognition analyses revealed genotype-specific patterns (Fig. 3A.). In GRN carriers, strong correlations were observed across bilateral regions, with the exception of the right lateral occipital cortex. C9orf72 carriers demonstrated widespread bilateral frontal correlations, with a broader distribution in the left hemisphere that extended into temporal and parietal cortices, resulting in reduced hemispheric symmetry compared with GRN. MAPT carriers showed the greatest hemispheric asymmetry: nearly all left-hemisphere regions exhibited strong cFW–CDR® plus NACC FTLD correlations, whereas right-hemisphere associations were weaker in the precentral gyrus, postcentral gyrus, supramarginal gyrus, occipital lobe, and cingulate gyrus.

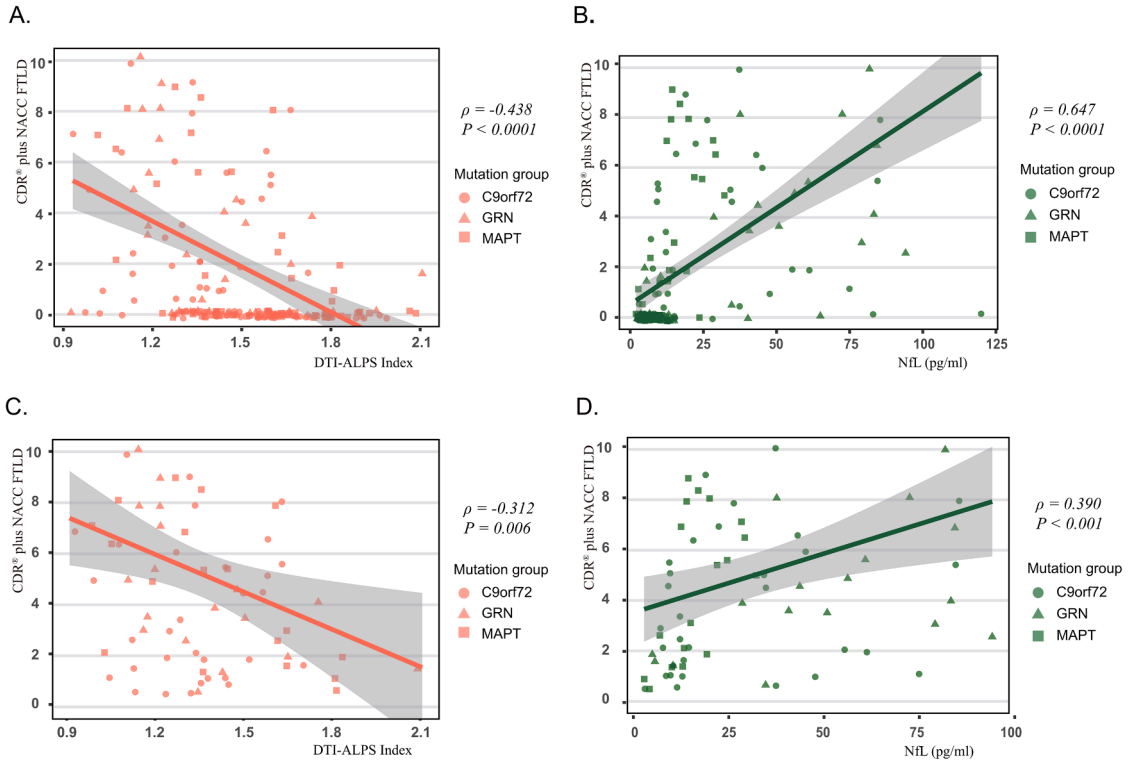

Fig. 2. Correlations of DTI-ALPS and NfL with clinical severity in the total FTLD cohort and symptomatic carriers Scatterplots show associations between DTI-ALPS or plasma neurofilament light chain (NfL) and CDR® plus NACC FTLD. A-B. show analyses in the total FTLD cohort, and C-D. show sensitivity analyses restricted to symptomatic carriers (Sx). Different point symbols indicate C9orf72, GRN, and MAPT mutation groups for visualization. Reported ρ and P-values correspond to Spearman correlation coefficients. Regression lines and 95% confidence intervals are shown for visualization and do not indicate mutation-specific regression. Regression lines represent the overall association within each analyzed sample and do not indicate mutation-specific regression.

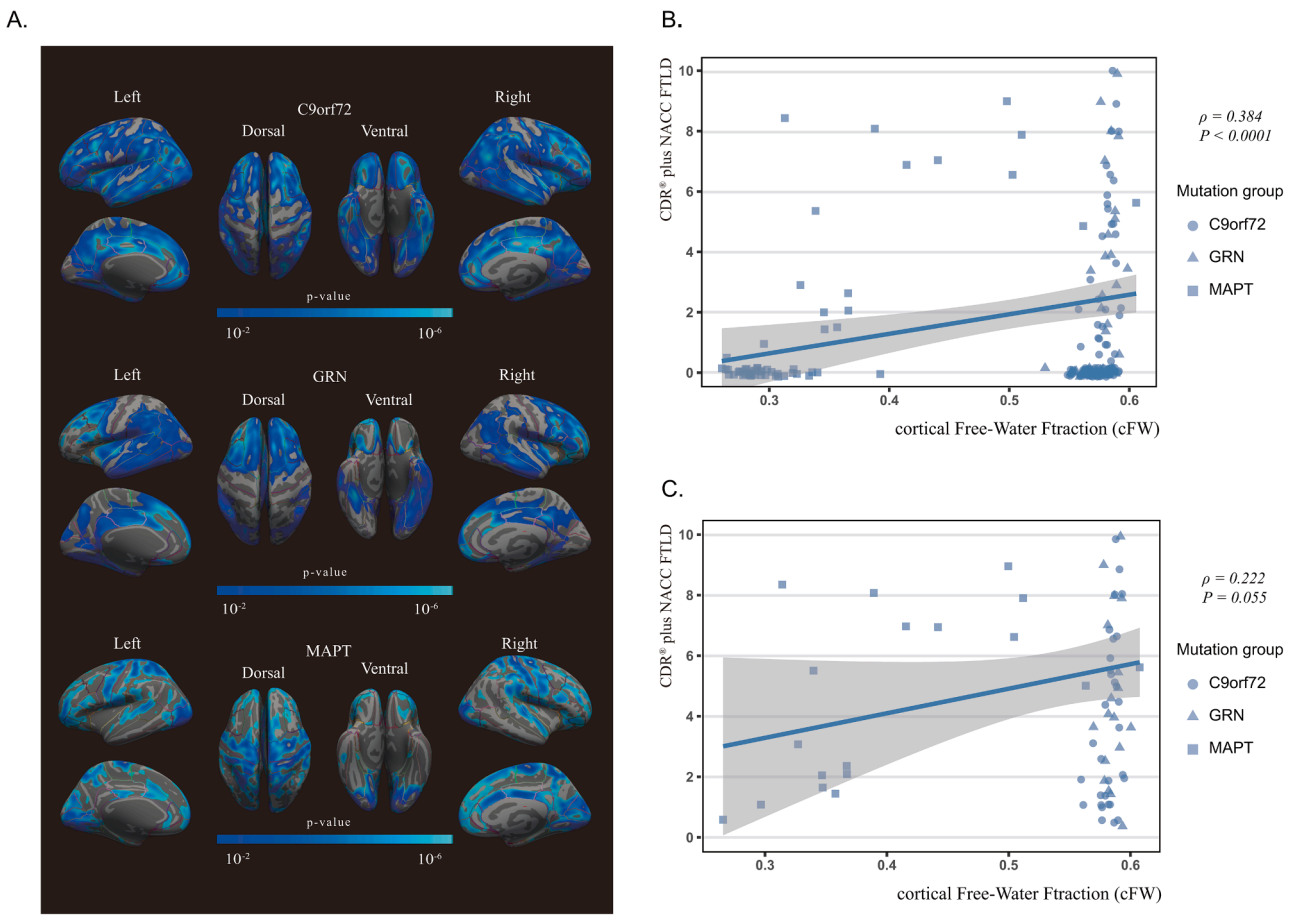

Fig. 3. Cortical distribution and global correlation of free water (cFW) with clinical severity in FTLD. A. Surface maps showing vertex-wise associations between cortical free-water fraction (cFW) and CDR® plus NACC FTLD within each FTLD mutation group. P-values are projected onto the left, right, dorsal, and ventral cortical surfaces. B–C. Partial correlations between cortical Free-Water (cFW) and FTLD Clinical Dementia Rating plus NACC FTLD (CDR® plus NACC FTLD) across all FTLD participants. B. Total group analysis; C. Symptomatic (Sx) participants only. Points are colored by mutation type: *C9orf72* (circles), *GRN* (triangles), *MAPT* (squares). Shaded areas represent 95% confidence intervals of the regression lines. Reported ρ and P-values correspond to Spearman correlation coefficients.

3.4. Mediation analysis of cFW, DTI-ALPS, and NfL in relation to cognition

We tested two sequential mediation models linking DTI-ALPS, cFW, plasma NfL, and cognition measured by the CDR® plus NACC FTLD. In the total FTLD cohort, both models showed a significant total effect of DTI-ALPS on CDR® plus NACC FTLD ($P < 0.001$) and a significant residual direct effect after accounting for the mediators ($P < 0.001$) (Fig. 4A-4B). In Sx-only analyses, the overall mediation pattern was broadly consistent, although cFW-related paths were attenuated (Fig. 4C-4D). Because Model B more directly isolated the NfL-mediated component linking DTI-ALPS to clinical severity, subsequent regional pathway-proportion analyses focused on Model B.

Across FTLD-vulnerable cortical regions, the Model B accounted for the largest proportion of the total indirect effect in both the total FTLD cohort and Sx carriers, whereas cFW-related and full serial pathways contributed smaller proportions. These findings identify plasma NfL as the dominant partial mediator among the tested pathways, while cFW provides additional region-specific information rather than serving as the principal mediator.

Regional mediation analyses further showed that the residual direct effect of DTI-ALPS on CDR® plus NACC FTLD remained significant across FTLD-vulnerable cortical regions after accounting for NfL and cFW. In parallel, the NfL-mediated pathway accounted for the largest proportion of the total indirect effect in Model B, whereas cFW-related and full serial pathways showed smaller, region-dependent contributions (Fig. 4E-4F; Supplementary Table S1–4). These findings support plasma NfL as the principal partial mediator of the DTI-ALPS clinical severity association, while the remaining direct effect suggests that additional mechanisms beyond NfL and cFW are also involved.

4. Discussion

This study systematically investigated the mechanistic links between glymphatic dysfunction, axonal injury, cortical microstructural alterations, and cognition in f-FTLD using multimodal biomarkers. By integrating DTI-ALPS, cFW, and plasma NfL, we provide convergent evidence for a cascade model evaluated across specific FTLD genetic subtypes. Three major findings emerged. First, reductions in DTI-ALPS and elevations in cFW were most pronounced in C9orf72 and GRN carriers, whereas MAPT carriers showed relatively lower cFW than C9orf72 and GRN carriers in the full carrier comparison, although cFW was also elevated among MAPT symptomatic carriers. Second, lower DTI-ALPS and higher NfL levels were associated with greater disease severity, with NfL showing the strongest association among the tested biomarkers. Third, mediation analyses demonstrated that the NfL-mediated component accounted for the largest proportion of the indirect pathway linking DTI-ALPS to clinical severity. However, the full serial pathway through cFW was not the dominant component, and a residual direct effect of DTI-ALPS remained, suggesting that additional biological mechanisms are likely involved. This overall pattern was broadly preserved in symptomatic carriers, although cFW related

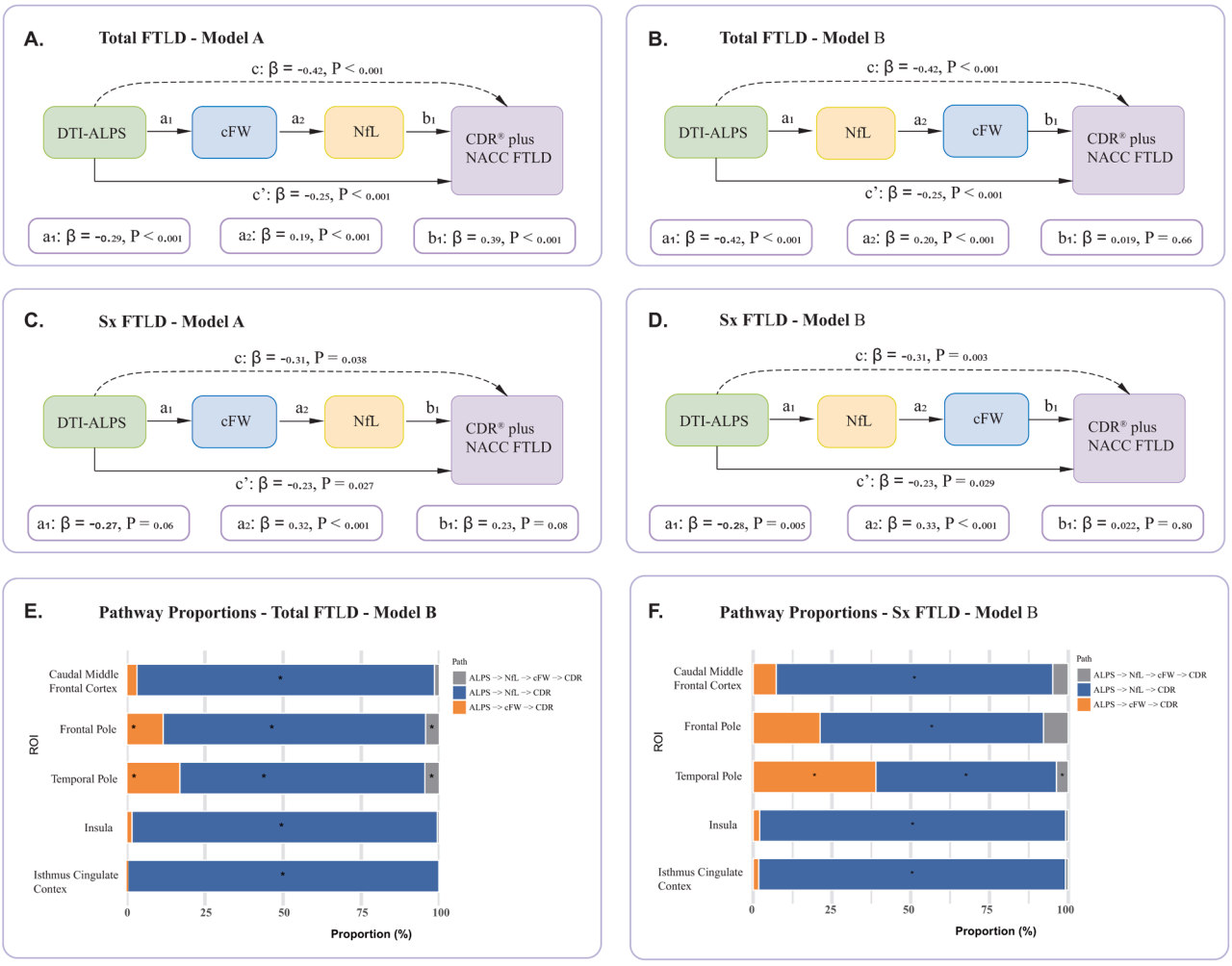

Fig. 4. Mediation models linking DTI-ALPS, plasma NfL, cFW, and clinical severity in the total FTLD cohort and symptomatic carriers. A–B: Serial mediation models in the total FTLD cohort. A. shows Model A, in which DTI-ALPS was modeled to affect CDR® plus NACC FTLD through cFW followed by plasma NfL. B. shows Model B, in which DTI-ALPS was modeled to affect CDR® plus NACC FTLD through plasma NfL followed by cFW. C–D: Corresponding serial mediation models in symptomatic mutation carriers (Sx). C. shows Model A and D. shows Model B in the Sx subgroup. Path coefficients are standardized estimates. Solid arrows indicate direct paths included in the mediation models, and dashed arrows indicate total effects. E–F.: Relative contributions of the three indirect pathways to the total indirect effect across FTLD-vulnerable cortical regions in Model B. E. shows pathway proportions in the total FTLD cohort, and F. shows pathway proportions in Sx carriers. CDR refers to CDR® plus NACC FTLD. Proportions were calculated as the absolute value of each indirect effect divided by the sum of the absolute values of all indirect effects within each ROI. Asterisks indicate indirect effects with bootstrap 95% confidence intervals not crossing zero.
Abbreviations: DTI-ALPS, diffusion tensor image analysis along the perivascular space; cFW, cortical free-water fraction; NfL, plasma neurofilament light chain; CDR, Clinical Dementia Rating; FTLD, frontotemporal lobar degeneration; Sx, symptomatic mutation carriers; ROI, region of interest.

associations were attenuated. This mediation pattern was broadly preserved when analyses were repeated in Sx group, suggesting that the main biomarker relationships were not driven solely by Pre-Sx participants.

4.1. *Partial mediation by NfL and additional non-NfL mechanisms*

A central finding of this study is that plasma NfL serves as an important partial mediator linking impaired glymphatic function to cognitive decline in f-FTLD. Reductions in DTI-ALPS were consistently associated with elevated NfL, which explained most of the indirect effect of DTI-ALPS on CDR® plus NACC FTLD scores. In contrast, cFW played a more modest and regionally restricted role across FTLD-vulnerable regions, suggesting that cortical free-water alterations provide complementary but less dominant information than plasma NfL in the DTI-ALPS-cognition pathway. Lower DTI-ALPS localized to anterior and FTLD-vulnerable networks, including frontal, temporal, insular, and cingulate regions, and tracked worse CDR® plus NACC FTLD, with plasma NfL emerging as the strongest correlate. These results suggest that systemic neuroaxonal injury, captured by plasma NfL, is a more proximate driver of clinical progression than localized microstructural alterations reflected by cFW.

Although plasma NfL emerged as the strongest mediator among the tested pathways, it did not fully account for the association between DTI-ALPS and CDR® plus NACC FTLD. The persistence of a direct effect suggests that glymphatic dysfunction may influence clinical severity through additional mechanisms beyond measurable axonal injury. These may include synaptic dysfunction, astroglial–vascular alterations, neuroinflammation, impaired clearance of disease-related proteins, or region-specific cortical microstructural changes not fully captured by global cFW or plasma NfL. Thus, rather than representing a complete explanatory pathway, the ALPS-NfL-cognition association should be interpreted as one major component of a broader multimodal cascade. Accordingly, prioritizing Model B should not be interpreted as excluding Model A or other biological pathways; rather, Model B was emphasized because it best captured the consistent NfL-mediated association

between DTI-ALPS and clinical severity.

Our mediation analyses highlight NfL as the strongest partial mediator among the tested pathways, whereas cFW contributed more modestly. This interpretation is consistent with previous studies reporting that reduced DTI-ALPS indices correlate with elevated plasma NfL levels and accelerated clinical progression in genetic FTLD [20]. Similarly, studies in behavioral variant FTD have demonstrated that regional glymphatic impairment, particularly in anterior brain regions, correlates with both NfL elevations and cognitive severity [13]. These converging findings suggest that impaired clearance accelerates axonal degeneration, which is sensitively captured by NfL.

By contrast, the limited mediating role of cFW in our analyses suggests that it reflects focal cortical microstructural disruption rather than a systemic pathway of neurodegeneration. Supporting this view, subtype-specific imaging studies have shown that cFW elevations are closely related to regional glymphatic dysfunction and vascular–astrocytic pathology but do not consistently explain global cognitive decline [12,32]. Recent evidence from Alzheimer's disease cohorts further extends this interpretation: Xu et al. demonstrated that choroid plexus free water fraction (CP FWf) is strongly associated with impaired DTI-ALPS, tau burden, GFAP elevations, synaptic loss, and cognitive impairment, and that its cognitive effects are mediated through tau and astrocytic activation rather than NfL [33]. Within this framework, the relative sparing of cFW in MAPT carriers may reflect tau-driven synaptic and neuronal dysfunction that does not produce widespread extracellular fluid shifts, whereas the marked FW increases in TDP-43–related *C9orf72* and *GRN* disease are consistent with greater astroglial–vascular involvement [14]. Collectively, these findings suggest that NfL and FW provide complementary but distinct insights into the glymphatic–axonal cascade: NfL indexing global neuroaxonal injury, and FW capturing additional pathological pathways involving astrocytic activation and tau accumulation.

4.2. Stage-specific robustness of the DTI-ALPS-NfL-clinical severity association

A further strength of the present study is that the major biomarker associations were examined not only in the total FTLD cohort but also after restricting the analyses to symptomatic mutation carriers. This stage-specific analysis is important because familial FTLD cohorts often include both pre-symptomatic and symptomatic individuals, and clinical severity measured by the CDR® plus NACC FTLD may differ substantially across these stages [23]. In the Sx-only analyses, lower DTI-ALPS remained significantly associated with greater clinical severity, and plasma NfL also remained positively associated with CDR® plus NACC FTLD scores. These findings suggest that the DTI-ALPS–NfL–clinical severity relationship was not simply driven by the separation between pre-symptomatic and symptomatic carriers, but persisted within the clinically affected stage. This result is consistent with prior evidence indicating that impaired glymphatic function is detectable in genetic and behavioral-variant frontotemporal dementia and is related to disease burden and neurodegenerative severity [13,20].

By contrast, the association between cFW and clinical severity was attenuated and no longer reached statistical significance in Sx carriers. This does not necessarily weaken the biological relevance of cFW, but rather suggests that cortical free-water alterations may be more spatially heterogeneous and more dependent on regional vulnerability, mutation subtype, or disease stage than DTI-ALPS and plasma NfL. Previous diffusion MRI studies have shown that free-water metrics are sensitive to subtle microstructural alterations and may provide complementary information beyond conventional atrophy measures, but their clinical associations can vary by brain region and disease context [18,32,34]. Therefore, the Sx findings refine the interpretation of our multimodal model: DTI-ALPS and NfL appear to reflect a relatively stable disease-severity-related pathway across clinical stages, whereas cFW may represent a more regionally constrained and subtype-dependent component of the broader glymphatic–neurodegenerative cascade.

4.3. Genotype-specific heterogeneity: stronger perivascular signatures in C9orf72/GRN than MAPT

Our mutation-specific findings are broadly consistent with prior work indicating stronger astroglial–vascular and perivascular involvement in TDP-43–related C9orf72/GRN disease than in MAPT-associated tauopathy: studies of C9orf72/GRN link perivascular dysfunction to extracellular fluid expansion, while MAPT cohorts often show less pronounced free-water changes for a given clinical severity [35,36]. They also align with evidence that FW metrics capture regionally circumscribed processes rather than uniform global decline [32]. What differs here is that we quantify these contrasts within a single framework that also includes the ALPS→NfL→cognition pathway: *C9orf72/GRN* exhibit the lowest DTI-ALPS and the most widespread cFW, whereas MAPT shows relative cFW sparing despite comparable clinical status. These divergences likely reflect design and methods—namely, a genetically defined cohort with mutation-specific analyses, multi-site diffusion harmonized with ComBat, rater-verified DTI-ALPS ROIs, and surface-based cFW sampling—which together increase sensitivity to perivascular signatures and reduce site/registration variance. Where findings parallel earlier reports, our study improves on them by anatomically localizing genotype differences, integrating imaging and fluid biomarkers rather than treating them separately, and embedding the comparisons in a quantitative, genotype-aware framework. Uniquely, we provide a **g**enotype-aware biomarker hierarchy: in TDP-43–related *C9orf72/GRN*, DTI-ALPS and NfL serve as primary readouts of perivascular failure and downstream axonal injury, while cFW highlights regional disease burden; in *MAPT* carriers, tau- and synapse-focused measures may be more sensitive than cFW, yielding testable predictions for longitudinal change and future trial enrichment [37,38].

4.4. Clinical and imaging correlates: anatomical localization and translational implications

Lower DTI-ALPS showed prominent involvement of anterior cortical regions and tracked worse CDR® plus NACC FTLD, with plasma NfL emerging as the strongest correlate. This topography is consistent with prior reports that anterior glymphatic impairment relates to both NfL elevations and clinical severity in bvFTD, and that effects concentrate in vulnerability hubs rather than distribute uniformly across the cortex. cFW contributed additional, regional information—most prominently in the middle temporal gyrus—aligning with evidence that FW metrics reflect focal astroglial and perivascular processes rather than system-wide decline [32,33].

4.5. Clinical and translational implications: toward genotype-aware biomarker panels and trials

These findings highlight NfL as a key translational biomarker that not only reflects axonal injury but also captures downstream effects of glymphatic dysfunction. FW provides complementary, region- and genotype-specific information, particularly in TDP-43–related subtypes. Together, DTI-ALPS, NfL, and cFW offer a multidimensional framework for early detection, participant selection, and monitoring therapeutic response in f-FTLD.

4.6. Limitations and scope of inference

Strengths include the large genetically defined cohort, harmonized multicenter diffusion data, integration of imaging with plasma biomarkers, and region-specific mediation models. Limitations include the cross-sectional design, single-b-value FW estimation, and modest sample sizes in *GRN* and *MAPT* subgroups. Longitudinal and multi-shell

diffusion studies, as well as pathological validation, are needed to establish causality and refine the mechanistic model [18,39,40].

4.7. Future directions and falsifiable predictions: longitudinal change, multi-shell diffusion, and multimodal integration (tau-PET/GFAP)

Future directions and falsifiable predictions should focus on validating the proposed cascade in longitudinal cohorts. Specifically, if impaired perivascular diffusivity (low DTI-ALPS) indeed precedes neuroaxonal injury and extracellular fluid expansion, we predict that longitudinal decline in DTI-ALPS will temporally precede increases in NfL and cFW, ultimately forecasting faster clinical progression. Multi-shell diffusion acquisitions may further refine free-water estimates by reducing model degeneracy and enhancing sensitivity to extracellular water. Integration with multimodal markers—such as tau-PET for tauopathy and plasma/CSF GFAP for astroglial reactivity—will allow dissection of pathway-specific mechanisms and clarify whether perivascular dysfunction is preferentially linked to TDP-43–related disease versus tauopathies. These falsifiable predictions offer testable hypotheses for ongoing natural history studies and provide a translational bridge toward biomarker-driven trials.

5. Conclusion

This study identifies plasma NfL as an important partial mediator of the association between glymphatic dysfunction and cognitive decline in f-FTLD, while cFW provides complementary region-specific information. The persistence of residual effects suggests that additional mechanisms beyond NfL-mediated axonal injury also contribute to cognitive impairment. These findings support a multimodal cascade model in which glymphatic dysfunction is linked to cognition through both axonal injury and other regionally or biologically distinct pathological processes.

Ethics approval and consent to participate

The study was approved by the institutional review boards at each participating center. All participants provided written informed consent prior to enrollment, in accordance with the Declaration of Helsinki. Genetic testing, neuroimaging procedures, and clinical assessments were conducted in compliance with ethical guidelines, ensuring participant confidentiality and the protection of personal data.

Declaration of generative AI and AI-assisted technologies in the writing process

I have not used any AI at all.

Funding statement

Major Scientific Research Project of the Department of Education of Anhui Province (No. 2024AH040242). High-level Talent Recruitment Program of Wannan Medical College (No. EYR202306). 2024 New Technology, New Project, New Service Program of the Second Affiliated Hospital of Wannan Medical College (No. Y24035), and Program for Excellent Sci-tech Innovation Teams of Anhui Provincial Department of Education (No. 2025AHGXZK10040).

CRediT authorship contribution statement

Meiling Qiu: Writing – original draft, Formal analysis. **Li Ding:** Writing – original draft, Formal analysis. **Rui Bao:** Writing – review & editing, Formal analysis. **Juanyu Gong:** Writing – review & editing, Formal analysis. **Wencai Ding:** Writing – review & editing, Supervision, Project administration. **Zhiding Shao:** Writing – review & editing, Supervision, Project administration. **Yongsheng Han:** Writing – review & editing, Supervision, Project administration.

Declaration of competing interest

All authors declare no conflicts of interest.

Acknowledgement statement

Data collection and dissemination of the data presented in this manuscript was supported by the ALLFTD Consortium (U19: AG063911, funded by the National Institute on Aging and the National Institute of Neurological Diseases and Stroke) and the former ARTFL & LEFFTDS Consortia (ARTFL: U54 NS092089, funded by the National Institute of Neurological Diseases and Stroke and National Center for Advancing Translational Sciences; LEFFTDS: U01 AG045390, funded by the National Institute on Aging and the National Institute of Neurological Diseases and Stroke). The authors acknowledge the invaluable contributions of the study participants and families and the assistance of the support staff at each of the participating sites.

Supplementary materials

Supplementary material associated with this article can be found, in the online version, at doi:10.1016/j.tjpad.2026.100639.

References

[1] Onyike CU, Diehl-Schmid J. The epidemiology of frontotemporal dementia (in eng) Int Rev Psychiatry 2013;25(2):130–7. https://doi.org/10.3109/09540261.2013.776523.
[2] Ren P, et al. Regional transcriptional vulnerability to basal forebrain functional dysconnectivity in mild cognitive impairment patients (in eng) Neurobiol Dis 2023;177:105983. https://doi.org/10.1016/j.nbd.2022.105983.
[3] Ding W, et al. Association of cortical and subcortical microstructure with disease severity: impact on cognitive decline and language impairments in frontotemporal lobar degeneration (in eng) Alzheimers Res Ther 2023;15(1):58. https://doi.org/10.1186/s13195-023-01208-7.
[4] Wood EM, et al. Development and validation of pedigree classification criteria for frontotemporal lobar degeneration (in eng) JAMA Neurol 2013;70(11):1411. https://doi.org/10.1001/jamaneurol.2013.3956.
[5] Iliff JJ, et al. A paravascular pathway facilitates CSF flow through the brain parenchyma and the clearance of interstitial solutes, including amyloid β (in eng) Sci Transl Med 2012;4(147):147ra111. https://doi.org/10.1126/scitranslmed.3003748. Aug 15.
[6] Staffaroni AM, et al. Rates of brain atrophy across disease stages in familial frontotemporal dementia associated with MAPT, GRN, and C9orf72 pathogenic variants (in eng) JAMA Netw Open 2020;3(10):e2022847. https://doi.org/10.1001/jamanetworkopen.2020.22847.
[7] Wang L, et al. Cortical microstructure in familial frontotemporal dementia associated with MAPT, GRN, and C9orf72 pathogenic variants: looking beyond atrophy (in eng) J Prev Alzheimers Dis 2025;12:100306. https://doi.org/10.1016/j.tjpad.2025.100306.
[8] Rasmussen MK, Mestre H, Nedergaard M. The glymphatic pathway in neurological disorders (in eng) Lancet Neurol 2018;17(11):1016–24. https://doi.org/10.1016/s1474-4422(18)30318-1.
[9] Kress BT, et al. Impairment of paravascular clearance pathways in the aging brain (in eng) Ann Neurol 2014;76(6):845–61. https://doi.org/10.1002/ana.24271.
[10] Ishida K, et al. Glymphatic system clears extracellular tau and protects from tau aggregation and neurodegeneration (in eng) J Exp Med 2022;219(3). https://doi.org/10.1084/jem.20211275.
[11] Eide PK, Vatnehol SAS, Emblem KE, Ringstad G. Magnetic resonance imaging provides evidence of glymphatic drainage from human brain to cervical lymph nodes. Sci Rep 2018;8(1):7194. https://doi.org/10.1038/s41598-018-25666-4.
[12] Chu M, et al. Glymphatic activity in behavioral variant frontotemporal dementia: link with vascular function and astrocytic activation (in eng) Alzheimers Dement 2025;21(8):e70561. https://doi.org/10.1002/alz.70561.
[13] Jiang D, et al. Regional glymphatic abnormality in behavioral variant frontotemporal dementia (in eng) Ann Neurol 2023;94(3):442–56. https://doi.org/10.1002/ana.26710.
[14] Xiao D, et al. Association of cortical morphology, white matter hyperintensity, and glymphatic function in frontotemporal dementia variants (in eng) Alzheimers Dement 2024;20(9):6045–59. https://doi.org/10.1002/alz.14158.
[15] Shao Z, Gao X, Cen S, Tang X, Gong J, Ding W. Unveiling the link between glymphatic function and cortical microstructures in post-traumatic stress disorder (in eng) J Affect Disord 2024;365:341–50. https://doi.org/10.1016/j.jad.2024.08.094.
[16] Taoka T, et al. Evaluation of glymphatic system activity with the diffusion MR technique: diffusion tensor image analysis along the perivascular space (DTI-ALPS)

in Alzheimer's disease cases (in eng) Jpn J Radiol 2017;35(4):172–8. https://doi.org/10.1007/s11604-017-0617-z.
[17] Ofori E, et al. Free-water imaging of the hippocampus is a sensitive marker of Alzheimer's disease (in eng) Neuroimage Clin 2019;24:101985. https://doi.org/10.1016/j.nicl.2019.101985.
[18] Sathe A, et al. Free-water: a promising structural biomarker for cognitive decline in aging and mild cognitive impairment (in eng) Imaging Neurosci (Camb) 2024;2:1–16. https://doi.org/10.1162/imag_a_00293.
[19] Wang X, Shi Z, Qiu Y, Sun D, Zhou H. Peripheral GFAP and NfL as early biomarkers for dementia: longitudinal insights from the UK Biobank (in eng) BMC Med 2024;22(1):192. https://doi.org/10.1186/s12916-024-03418-8.
[20] Premi E, et al. Impaired glymphatic system in genetic frontotemporal dementia: a GENFI study (in eng) Brain Commun 2024;6(4):fcae185. https://doi.org/10.1093/braincomms/fcae185.
[21] Boeve B, et al. The longitudinal evaluation of familial frontotemporal dementia subjects protocol: framework and methodology (in eng) Alzheimers Dement 2020;16(1):22–36. https://doi.org/10.1016/j.jalz.2019.06.4947.
[22] Ramos EM, et al. Genetic screening of a large series of North American sporadic and familial frontotemporal dementia cases (in eng) Alzheimers Dement 2020;16(1):118–30. https://doi.org/10.1002/alz.12011.
[23] Olney NT, et al. Clinical and volumetric changes with increasing functional impairment in familial frontotemporal lobar degeneration (in eng) Alzheimers Dement 2020;16(1):49–59. https://doi.org/10.1016/j.jalz.2019.08.196.
[24] Schilling KG, et al. Synthesized b0 for diffusion distortion correction (Synb0-DisCo) (in eng) Magn Reson Imaging 2019;64:62–70. https://doi.org/10.1016/j.mri.2019.05.008.
[25] Pasternak O, Sochen N, Gur Y, Intrator N, Assaf Y. Free water elimination and mapping from diffusion MRI (in eng) Magn Reson Med 2009;62(3):717–30. https://doi.org/10.1002/mrm.22055.
[26] Maillard P, et al. MRI free water as a biomarker for cognitive performance: validation in the MarkVCID consortium (in eng) Alzheimers Dement 2022;14(1):e12362. https://doi.org/10.1002/dad2.12362.
[27] Greve DN, Fischl B. Accurate and robust brain image alignment using boundary-based registration (in eng) Neuroimage 2009;48(1):63–72. https://doi.org/10.1016/j.neuroimage.2009.06.060.
[28] Seeley WW. Anterior insula degeneration in frontotemporal dementia (in eng) Brain Struct Funct 2010;214(5–6):465–75. https://doi.org/10.1007/s00429-010-0263-z.
[29] Fumagalli GG, et al. Distinct patterns of brain atrophy in genetic frontotemporal dementia initiative (GENFI) cohort revealed by visual rating scales (in eng) Alzheimers Res Ther 2018;10(1):46. https://doi.org/10.1186/s13195-018-0376-9.
[30] Cash DM, et al. Patterns of gray matter atrophy in genetic frontotemporal dementia: results from the GENFI study (in eng) Neurobiol Aging 2018;62:191–6. https://doi.org/10.1016/j.neurobiolaging.2017.10.008.
[31] Fortin JP, et al. Harmonization of multi-site diffusion tensor imaging data (in eng) Neuroimage 2017;161:149–70. https://doi.org/10.1016/j.neuroimage.2017.08.047.
[32] Arighi A, et al. Aquaporin-4 cerebrospinal fluid levels are higher in neurodegenerative dementia: looking at glymphatic system dysregulation (in eng) Alzheimers Res Ther 2022;14(1):135. https://doi.org/10.1186/s13195-022-01077-6.
[33] Xu X, et al. Choroid plexus free-water correlates with glymphatic function in Alzheimer's disease (in eng) Alzheimers Dement 2025;21(5):e70239. https://doi.org/10.1002/alz.70239.
[34] Xu X, et al. Choroid plexus free-water correlates with glymphatic function in Alzheimer's disease. Alzheimer's Dement 2025;21(5):e70239. https://doi.org/10.1002/alz.70239.
[35] Neumann M, et al. Ubiquitinated TDP-43 in frontotemporal lobar degeneration and amyotrophic lateral sclerosis (in eng) Science 2006;314(5796):130–3. https://doi.org/10.1126/science.1134108.
[36] Martens LH, et al. Progranulin deficiency promotes neuroinflammation and neuron loss following toxin-induced injury (in eng) J Clin Invest 2012;122(11):3955–9. https://doi.org/10.1172/jci63113.
[37] DeVos SL, et al. Tau reduction prevents neuronal loss and reverses pathological tau deposition and seeding in mice with tauopathy (in eng) Sci Transl Med 2017;9(374). https://doi.org/10.1126/scitranslmed.aag0481.
[38] Levy JP, et al. 18F-MK-6240 tau-PET in genetic frontotemporal dementia (in eng) Brain 2022;145(5):1763–72. https://doi.org/10.1093/brain/awab392.
[39] Hsu JL, et al. Magnetic resonance images implicate that glymphatic alterations mediate cognitive dysfunction in Alzheimer disease (in eng) Ann Neurol 2023;93(1):164–74. https://doi.org/10.1002/ana.26516.
[40] Zhao S, et al. Cognitive impairment and vulnerability of cholinergic brain network in the Alzheimer's continuum: free-water imaging based on diffusion tensor imaging (in eng) Front Neurosci 2025;19:1587702. https://doi.org/10.3389/fnins.2025.1587702.